

To appear in *The Astrophysical Journal, Letters*

## Inverse Depolarization: A Potential Probe of Internal Faraday Rotation and Helical Magnetic Fields in Extragalactic Radio Jets

D. C. Homan

*Department of Physics and Astronomy, Denison University, Granville, OH 43023;*  
*homand@denison.edu*

### ABSTRACT

Motivated by recent observations that show increasing fractional linear polarization with increasing wavelength in a small number of optically thin jet features, i.e. “inverse depolarization”, we present a physical model that can explain this effect and may provide a new and complementary probe of the low energy particle population and possible helical magnetic fields in extragalactic radio jets. In our model, structural inhomogeneities in the jet magnetic field create cancellation of polarization along the line of sight. Internal Faraday rotation, which increases like wavelength squared, acts to align the polarization from the far and near sides of the jet, leading to increased polarization at longer wavelengths. Structural inhomogeneities of the right type are naturally produced in helical magnetic fields and will also appear in randomly tangled magnetic fields. We explore both alternatives and find that, for random fields, the length scale for tangling cannot be too small a fraction of the jet diameter and still be consistent with the relatively high levels of fractional polarization observed in these features. We also find that helical magnetic fields naturally produce transverse structure for inverse depolarization which may be observable even in partially resolved jets.

*Subject headings:* galaxies: active — galaxies: jets — radiation mechanisms: non-thermal — radio continuum: galaxies — quasars: general — BL Lacertae objects: general

### 1. Introduction

Faraday rotation, the rotation of the plane of linearly polarized radiation propagating through a magnetized plasma, has long been thought not to play an important role *internal* to extragalactic radio jets, in large part because the depolarization and divergence from a pure  $\lambda^2$  rotation law expected due to large amounts of internal rotation (Burn 1966) have not been clearly observed; however, detecting this behavior in real sources can be difficult (Cioffi & Jones 1980). Observations of circularly polarized radiation have suggested that Faraday rotation may indeed operate internal

to jets to drive the conversion of linear polarization into circular (e.g. Wardle & Homan 2003; Homan et al. 2009). Additionally, observations of variations in Faraday rotation and transverse structure, or gradients, in rotation measure have indicated that some Faraday screens lie very close to the jet, perhaps in a boundary layer around it that may contain helical magnetic fields (e.g. Asada et al. 2002; Gabuzda et al. 2004; Zavala & Taylor 2005; Gómez et al. 2011; Kronberg et al. 2011). The observation and interpretation of transverse rotation measure gradients as evidence for helical fields remains controversial (Taylor & Zavala 2010; Broderick & McKinney 2010). Given the central role helical fields are believed to play in collimating and accelerating jets near their origin from the super massive black hole–accretion disk system (e.g. Meier et al. 2001), it is important to pursue additional observational signatures of helical magnetic fields in jets (Lyutikov et al. 2005; Marscher et al. 2008; Clausen-Brown et al. 2011; Porth et al. 2011).

An intriguing phenomenon has recently been observed in multiple optically thin jet features in the blazars 3C 273, 3C 454.3, and a single jet feature in the blazar 1514–241. Hovatta et al. (2012, submitted) have measured increasing polarization with increasing wavelength in their Very Long Baseline Array observations of these jet features at  $\lambda\lambda$  2.0, 2.5, 3.6, and 3.7 cm. The observed increases range from factors of  $\sim 1.5$  up to  $\sim 3$  times over this wavelength range. Homan et al. (2002) saw a similar increase in fractional polarization of up to a factor of two in a jet feature in 3C 120 between  $\lambda\lambda$  1.3 and 2.0 cm. The jet features involved in these cases are relatively strongly polarized at their maximum wavelength, with fractional polarization ranging from 5 to more than 20 percent. The effect can apparently vary with epochs separated by a few months, although it is clearly observed for two epochs spanning three months in two features in 3C 273 (Hovatta et al. 2012, submitted) and over four epochs spanning six months in the jet feature in 3C 120 (Homan et al. 2002).

The sense of this effect is the opposite of that normally expected for Faraday depolarization where fractional polarization decreases with increasing wavelength, and we therefore term it “inverse depolarization”. Increasing fractional polarization with wavelength might naturally arise in the unresolved, optically thick core region where one is observing different parts of the jet at different wavelengths (e.g. Konigl 1981), but the jet features showing this effect are (1) well separated from the core in the optically thin part of the jet and (2) reasonably isolated from other strong jet features (Hovatta et al. 2012, submitted). In this letter we propose an alternative explanation which combines structural inhomogeneities in the jet magnetic field along the line of sight with *internal* Faraday rotation to produce an inverse depolarization effect in optically thin jet features<sup>1</sup>. If our explanation is correct, observed inverse depolarization is evidence of internal Faraday rotation in jets and may prove to be a powerful and complementary tool to rotation measure studies of jet magnetic fields and particles, including helical field geometries.

---

<sup>1</sup>A similar effect due to Faraday conversion of linear to circular polarization was seen in simulations by Baldwin & Homan (2009) at modest optical depths,  $\tau \simeq 0.1 - 1.0$ , while the mechanism proposed here can operate in optically thin regions and requires only internal Faraday rotation.

Our model for inverse depolarization is presented in §2 and applied to both helical field geometries and randomly tangled magnetic fields. §3 discusses these results and the prospects for using this effect to study the magnetic field geometry of extragalactic jets.

## 2. Model for Inverse Depolarization

In the subsections that follow, we present a simple model for generating inverse depolarization, i.e. increasing polarization with increasing wavelength, in radio jets at low optical depth,  $\tau \ll 1$ . Our model combines *internal* Faraday rotation with structural differences in the magnetic field between the far and near sides of the jet. If the magnetic field structure naturally leads to low net polarization at short wavelengths, internal Faraday rotation can act to align polarization from the far side of the jet with polarization produced at the near side of the jet, reducing the cancellation between them and leading to increased net polarization at longer wavelengths.

We characterize the amount of internal rotation at a given wavelength by the Faraday depth,  $\tau_f$ , which is proportional to  $\lambda^2$ . Internal to the jet, Faraday depth may be due to either a population of thermal electrons or the low-energy end of the relativistic particle distribution (e.g. Jones & O’Dell 1977; Huang & Shcherbakov 2011), and we discuss these contributions in §2.5.

### 2.1. Linearly Polarized Transfer at Low Optical Depth

The radiative transfer equations for Stokes  $Q$  and  $U$  at low optical depth are given by the following expressions, assuming the projected magnetic field is purely east-west (Jones & O’Dell 1977; Jones 1988). Note that in the low optical depth limit, we have ignored the coupling of Stokes  $I$  and  $V$  to  $Q$  and  $U$

$$\frac{dQ}{d\tau} + Q + \zeta_V^* U = \epsilon J, \quad \frac{dU}{d\tau} + U - \zeta_V^* Q = 0 \quad (1)$$

The solutions to these equations<sup>2</sup>, including an initial polarization,  $P_0$  at angle  $\chi_0$  are

$$Q = \frac{\epsilon J}{(\tau_f/\tau)^2 + 1} \left[ 1 - e^{-\tau} \cos \tau_f + \left(\frac{\tau_f}{\tau}\right) e^{-\tau} \sin \tau_f \right] + P_0 e^{-\tau} \cos(2\chi_0 + \tau_f)$$

$$U = \frac{\epsilon J}{(\tau_f/\tau)^2 + 1} \left[ \left(\frac{\tau_f}{\tau}\right) (1 - e^{-\tau} \cos \tau_f) - e^{-\tau} \sin \tau_f \right] + P_0 e^{-\tau} \sin(2\chi_0 + \tau_f) \quad (2)$$

---

<sup>2</sup>The solutions to the general form were obtained with WolframAlpha, <http://www.wolframalpha.com/> and checked against numerical integration of the full equations of radiative transfer (Homan et al. 2009).

where  $\tau$  is the optical depth and  $\tau_f = \zeta_V^* \tau$  is the Faraday depth and is proportional to  $\lambda^2$  (e.g. Jones & O’Dell 1977; Cioffi & Jones 1980). Note that at low optical depth, Stokes  $I = J\tau$ . The final Stokes  $Q$  and  $U$  are used to compute the fractional polarization,  $m = \sqrt{Q^2 + U^2}/I$ , and electric vector position angle (EVPA),  $\chi = 0.5 \times \tan^{-1}(U/Q)$  of the emergent polarization.

## 2.2. Inverse Depolarization in a Simple Two-Cell System

We apply these expressions to a “two-cell” system along the line of sight. Each cell has an internal Faraday rotation of depth  $\tau_f/2$  for a total Faraday depth of  $\tau_f$  for the system. In addition to their common line-of-sight magnetic field, both cells also have a uniform magnetic field,  $B_\perp$ , in the plane of the sky. The field in the two cells differs only by a rotation on the sky of  $\Delta\phi$ . The  $B_\perp$  in the cell closest to the observer is taken to be purely East-West, while the field in the furthest cell differs in orientation by an offset angle,  $\Delta\phi$ , Northward from East. Note that positive Faraday depth will tend to rotate the  $\chi$  of the emitted radiation from North to East<sup>3</sup>.

Polarized radiation generated in the furthest cell must travel through the nearest cell to reach the observer. In the absence of internal Faraday rotation, the offset angle  $\Delta\phi$  will produce some cancellation between the polarization emitted from the far and near cells. For  $\Delta\phi = 90^\circ$ , this structural cancellation would be complete at short wavelengths.

Figure 1 shows the emergent polarization as a function of  $\tau_f$  ( $\propto \lambda^2$ ) for a range of  $\Delta\phi$  offsets. For  $\Delta\phi = 0$ , Burn (1966) depolarization in a slab geometry is reproduced. At larger offsets, partial cancellation of the emergent polarization is clear at  $\tau_f = 0$ , and for  $0 < \Delta\phi \leq 90^\circ$  the internal rotation initially begins to reverse this structural depolarization up to a certain limit until  $\tau_f$  becomes too large. For  $\Delta\phi > 90^\circ$  the internal rotation initially increases the depolarization as  $\tau_f$  increases but later can also go into a region of ‘inverse depolarization’.

Figure 1(b) shows that for simple field geometries, such as the two cell system shown here, the observed EVPA for internal rotation is linear in  $\lambda^2$  with  $\chi = \chi_0 + \tau_f/4$  with additional  $90^\circ$  flips when the polarized flux passes through zero<sup>4</sup> (e.g. Burn 1966). More complicated geometries which include a range of  $\tau_f$  values along different lines of sight are expected to diverge from a  $\lambda^2$  law after total rotations  $\gtrsim 45^\circ$  (Burn 1966), although the total rotation at which the non- $\lambda^2$  behavior becomes apparent will vary from case to case (see the lower panels of Figure 2 as examples).

---

<sup>3</sup>Negative Faraday depth would simply result in a rotation of  $\chi$  in the opposite direction.

<sup>4</sup>Note that for purely *external* rotation in a uniform screen  $\tau_f$  is also proportional to  $\lambda^2$ , but  $\chi = \chi_0 + \tau_f/2$ . However, that is not the case we consider in this paper.

### 2.3. Inverse Depolarization in Helical Fields

To evaluate the efficiency of this mechanism in a purely helical field geometry, we numerically solved the full equations of radiative transfer (Jones & O’Dell 1977; Jones 1988) for a variety of combinations of toroidal ( $f_t$ ) and uniform ( $f_u$ ) field components in an optically thin cylinder. The uniform field is poloidally directed along the jet axis and has constant magnitude throughout the cylindrical cross-section of the jet. The magnitude of the toroidal field component grows linearly with distance from the jet axis from 0 to  $f_t$  at the outside edge of the cylinder, consistent with field generated by a current which is carried uniformly in the jet volume. A more detailed description of the radiative transfer simulation and magnetic field parameters is given by Homan et al. (2009). The simulated jets are relativistic, with bulk Lorentz factor  $\Gamma = 10$ , and viewed at one-half the optimum angle for superluminal motion  $\theta = 1/2\Gamma$ . This intermediate viewing angle is the most probable in a flux-density limited sample (Lister & Marscher 1997); however, we note that a wide range of viewing angles is possible and may strengthen or weaken the inverse depolarization effect in various cases. Internal Faraday depth is provided by the low end of the relativistic particle spectrum<sup>5</sup>, resulting in  $\langle\tau_f\rangle \sim 2\lambda^2$ , averaged over all lines of sight, for the simulations shown in Figure 2.

Figure 2 plots the integrated polarization from the entire jet cross-section as a function of  $\lambda^2$  for a variety of combinations of  $f_u$  and  $f_t$ . Even in these integrated results, the inverse depolarization effect is clearly seen, for at least some range of wavelengths, in half of the cases shown. Note that there is not necessarily any correlation in the integrated results between the amount of inverse depolarization and the observed Faraday rotation (given in the lower panel of Figure 2). This lack of correlation in the integrated results is primarily due to variation in both Faraday depth and field order across the jet.

In a helical magnetic field, the offset angle,  $\Delta\phi$ , between the back and front of the jet varies with location along the cylindrical cross-section. Additionally, the internal Faraday depth,  $\tau_f$ , is produced by the line-of-sight components of *both* the poloidal (uniform) and toroidal fields. The contribution to  $\tau_f$  from the toroidal field will also vary with location along the cylindrical cross-section, changing the sign of its contribution at the mid-point of the jet. The details of how these factors combine depend on a variety of factors, but the important point is that in a helical magnetic field, the inverse depolarization effect can vary strongly as a function of location along the jet cross-section. Detecting and modeling this variation requires sensitive observations at several wavelengths; however, in Figure 3 we demonstrate that the effects could be observable even with only two beam-widths of resolutions across the jet.

Figure 3 shows a partially resolved, cylindrical jet cross-section in relative total intensity (solid curve) and fractional polarization at a range of wavelengths (symbols). Even with only two beam-

---

<sup>5</sup>We note that the same results would be obtained by introducing thermal particles to do the rotation, as it is only the amount of rotation along each line of sight that determines the emergent polarization.

widths of resolution, the inverse depolarization effect clearly varies with location along the jet, being extremely strong at the bottom of the jet (left of figure) and turning to normal depolarization at the top of the jet (right of figure). This is a particular case, and, as noted above, the details will vary depending on the combination of poloidal and toroidal fields, jet viewing angle, and average Faraday depth. It is interesting to note that a jet viewed perpendicular to its axis in the fluid frame,  $\theta = 1/\Gamma$ , can still have a significant inverse depolarization effect, even though it has no component of poloidal field along the line of sight. This can happen if the field crossing angle is  $\Delta\phi \simeq \pm 90^\circ$  above and below the jet axis. Although the  $\tau_f$  provided by the toroidal field reverses across the axis, either sign of  $\tau_f$  will increase the net polarization from near zero giving inverse depolarization on both the top and bottom of the jet.

#### 2.4. Inverse Depolarization in Random Fields

The structural inhomogeneities that are necessary for inverse depolarization can also be produced stochastically in a randomly tangled magnetic field. The effect should be strongest in those cases where structural cancellation leads to low net polarization so that internal rotation can effectively increase the fraction of polarization with wavelength. We have simulated this scenario with a  $N \times N \times N$  cube of cells, each with a randomly oriented magnetic field. The results for  $N = 5$  and  $N = 15$  are plotted in Figure 4 where we show the percentage of cases with significant inverse depolarization between two wavelengths (top panel) and the average polarization of those cases showing the inverse depolarization (bottom panel). Significant inverse depolarization occurs for 20 – 30% of cases for both  $N = 5$  and  $N = 15$ , with and without a modest “shock” applied to the entire cube (see caption), for a range of mean Faraday depths. However, the mean fractional polarization in the  $N = 15$  cases with inverse depolarization is very low,  $\simeq 1 - 2\%$ . The  $N = 5$  cases are larger,  $\simeq 5 - 8\%$  polarization, and more consistent with the levels of polarization seen in the jets showing this effect, although levels up to 20% are observed (Hovatta et al. 2012, submitted).

#### 2.5. Internal Faraday Depth

Internal to the jet, Faraday depth may be due to either a population of “cold” thermal electrons with number density,  $n_c$ , or the low-energy end of the relativistic particle distribution with number density,  $n_r$ . The relative contributions to the Faraday depth from the cold and relativistic particles are given by Jones & O’Dell (1977):

$$\frac{\tau_f^{(r)}}{\tau_f^{(c)}} = 2\alpha \frac{\alpha + 3/2}{\alpha + 1} \frac{\ln \gamma_i}{\gamma_i^2} \left( \frac{n_r}{n_c} \right) \quad (3)$$

where  $\alpha$  is the optically thin spectral index defined by  $S \propto \nu^{-\alpha}$ . The relativistic contribution as-

sumes a power-law distribution of particles with  $dn_r = K\gamma^{-(2\alpha+1)}d\gamma$  with a lower cutoff  $\gamma_i$ . For cold particles alone, we have the following familiar expression (in cgs units) (e.g. Rybicki & Lightman 1979).

$$\tau_f^{(c)} = \frac{e^3}{\pi m^2 c^4} \frac{\delta^2 \lambda^2}{(1+z)^2} \int n_c \mathbf{B} \cdot d\mathbf{l} \quad (4)$$

Note that  $\lambda$  in the above expression is the *observed* wavelength. Internal to the jet, the rotating plasma sees a much longer wavelength because the jet emission is Doppler boosted in the observer’s frame by factor,  $\delta/(1+z)$ . It is interesting to note that, for typical blazars with  $\delta \gtrsim 10$ , low-energy particles internal to the jet (whether cold or relativistic) can be hundreds of times more effective at Faraday rotation than rotating plasma external to the jet which is not moving relativistically in relation to the observer (assuming equivalent field strengths and path lengths).

The inverse depolarization effect proposed here requires only modest Faraday depths of order  $\tau_f \simeq$  a few, and indeed large Faraday depths would effectively depolarize jets, which is not observed in blazars. Suppression of large internal Faraday depths requires some combination of the following conditions: (1) low number density of the rotating particles, both thermal *and* low-energy relativistic, (2) pairing of low-energy relativistic electrons with low-energy relativistic positrons without a significant thermal component, or (3) a large number of magnetic field reversals along the line of sight. Study of this effect which implies modest but not large internal Faraday rotation, and provides constraints on the magnetic field order, may yield new information on the low-energy particle population of relativistic jets.

### 3. Summary and Conclusions

We have shown that observations of inverse depolarization in optically thin jet features (Hovatta et al. 2012, submitted; Homan et al. 2002), can potentially be explained by a simple physical model which combines structural inhomogeneities in the magnetic field along the line of sight with internal Faraday rotation. Structural inhomogeneities of the right type are naturally produced by helical magnetic fields. Random magnetic fields can also produce this effect, but must be tangled on long length scales in the jet to be consistent with the modest to high levels of fractional polarization observed in these features. Real jets likely contain some combination of randomly tangled and ordered field components (e.g. Hughes 2005; Laing et al. 2006); however, it is intriguing that 3 of the 4 jets which appear to show this effect also have transverse rotation measure gradients, a potential signature of helical magnetic fields (Asada et al. 2002; Zavala & Taylor 2005; Gómez et al. 2008; Hovatta et al. 2012, submitted), although for 3C 120 the evidence favors an interaction with the external medium as the source of the rotation measure gradient (Gómez et al. 2008). In the case of inverse depolarization produced by helical magnetic fields, we have demonstrated that the transverse structure of inverse depolarization could be measured even in partially resolved jets,

and the recently expanded bandwidth of the Very Long Baseline Array may allow highly sensitive, multi-wavelength observations of transverse jet profiles to test these predictions in the near future.

The author would like to thank John Wardle, Talvikki Hovatta, Matt Lister, Margo Aller and the other members of the MOJAVE collaboration for helpful discussions. This work has been supported by NSF grant AST-0707693

## REFERENCES

- Asada, K., Inoue, M., Uchida, Y., Kamenno, S., Fujisawa, K., Iguchi, S., & Mutoh, M. 2002, PASJ, 54, L39
- Baldwin, C., & Homan, D. C. 2009, Bulletin of the American Astronomical Society, 41, #422.10
- Broderick, A. E., & McKinney, J. C. 2010, ApJ, 725, 750
- Burn, B. J. 1966, MNRAS, 133, 67
- Cioffi, D. F., & Jones, T. W. 1980, AJ, 85, 368
- Clausen-Brown, E., Lyutikov, M., & Kharb, P. 2011, MNRAS, 415, 2081
- Gabuzda, D. C., Murray, É., & Cronin, P. 2004, MNRAS, 351, L89
- Gómez, J. L., Marscher, A. P., Jorstad, S. G., Agudo, I., & Roca-Sogorb, M. 2008, ApJ, 681, L69
- Gómez, J. L., Roca-Sogorb, M., Agudo, I., Marscher, A. P., & Jorstad, S. G. 2011, ApJ, 733, 11
- Homan, D. C., Lister, M. L., Aller, H. D., Aller, M. F., & Wardle, J. F. C. 2009, ApJ, 696, 328
- Homan, D. C., Ojha, R., Wardle, J. F. C., Roberts, D. H., Aller, M. F., Aller, H. D., & Hughes, P. A. 2002, ApJ, 568, 99
- Hovatta, T., Lister, M. L., Aller, M. F., Aller, H. D., Homan, D. C., Kovalev, Y. Y., Pushkarev, A. B., Savolainen, T. 2012, AJ, submitted
- Huang, L., & Shcherbakov, R. V. 2011, MNRAS, 416, 2574
- Hughes, P. A. 2005, ApJ, 621, 635
- Jones, T. W. 1988, ApJ, 332, 678
- Jones, T. W. & O’Dell, S. L. 1977, ApJ, 214, 522
- Konigl, A. 1981, ApJ, 243, 700
- Kronberg, P. P., Lovelace, R. V. E., Lapenta, G., & Colgate, S. A. 2011, ApJ, 741, L15



- Laing, R. A., Canvin, J. R., & Bridle, A. H. 2006, *Astronomische Nachrichten*, 327, 523
- Lister, M. L., & Marscher, A. P. 1997, *ApJ*, 476, 572
- Lyutikov, M., Pariev, V. I., & Gabuzda, D. C. 2005, *MNRAS*, 360, 869
- Marscher, A. P., et al. 2008, *Nature*, 452, 966
- Meier, D. L., Koide, S., & Uchida, Y. 2001, *Science*, 291, 84
- Porth, O., Fendt, C., Meliani, Z., & Vaidya, B. 2011, *ApJ*, 737, 42
- Rybicki, G. B., & Lightman, A. P. 1979, *Radiative Processes in Astrophysics* (New York, NY: Wiley-Interscience)
- Taylor, G. B., & Zavala, R. 2010, *ApJ*, 722, L183
- Wardle, J. F. C., Cawthorne, T. V., Roberts, D. H., & Brown, L. F. 1994, *ApJ*, 437, 122
- Wardle, J. F. C., & Homan, D. C. 2003, *Ap&SS*, 288, 143
- Zavala, R. T., & Taylor, G. B. 2005, *ApJ*, 626, L73

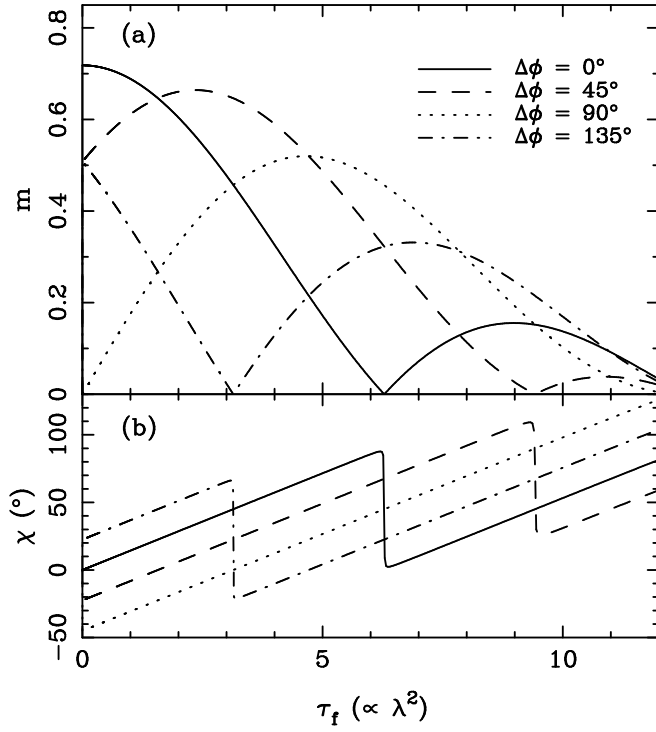


Fig. 1.— Plot of fractional linear polarization (top panel) and EVPA (bottom panel) as a function of Faraday depth,  $\tau_f \propto \lambda^2$ , for a simple two-cell system along the line of sight. Each line shows the emergent polarization for a different offset angle,  $\Delta\phi$ , for the projected magnetic field between the far and near cells.

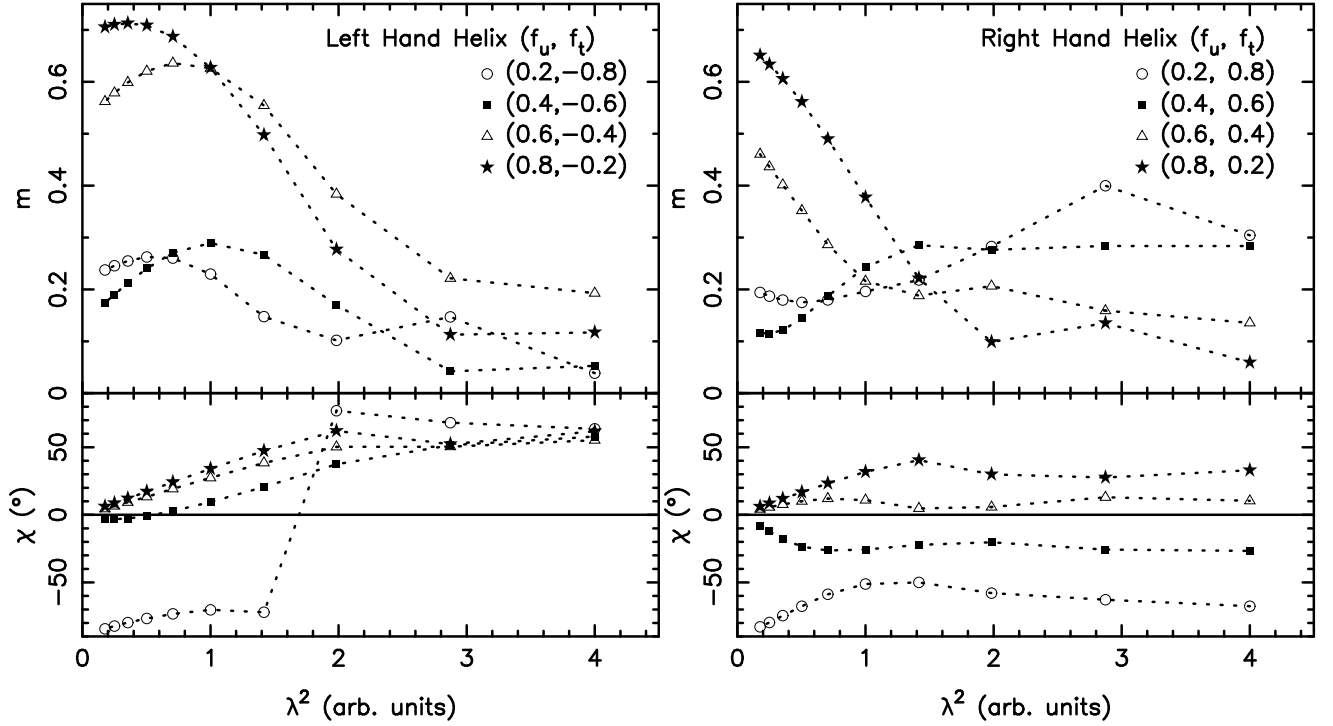


Fig. 2.— Integrated polarization as a function of  $\lambda^2$  for cylindrical jets with pure helical magnetic fields. Jets with various combinations of uniform magnetic field, along the jet axis,  $f_u$ , and toroidal magnetic field,  $f_t$  are plotted. All of the jets here are identical except for their  $(f_u, f_t)$  combination, and all are at an angle  $\theta = 1/2\Gamma$  to the observers line of sight, inside the optimum angle for superluminal motion.

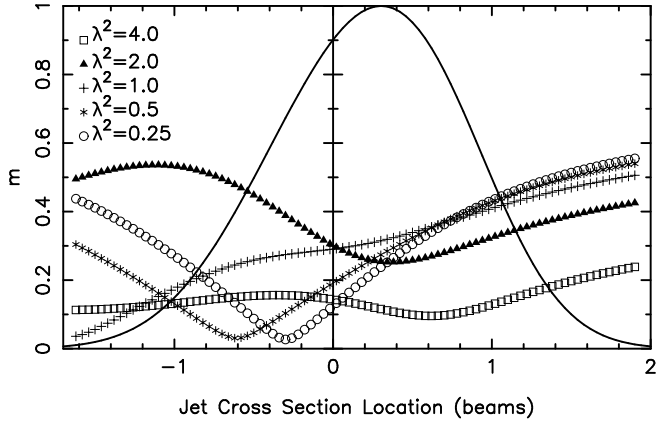


Fig. 3.— Fractional polarization,  $m$ , as a function of transverse jet position for a partially resolved jet where the jet diameter is twice the FWHM of the observing beam. The  $(f_u, f_t) = (0.4, -0.6)$  case from figure 2 is plotted for several values of  $\lambda^2$ . The single solid line represents the Stokes  $I$  intensity normalized to a maximum of 1.0. Note that the asymmetric profile in Stokes  $I$  is similar to that predicted by Clausen-Brown et al. (2011) for a helical magnetic field viewed at  $\theta = 1/2\Gamma$ .

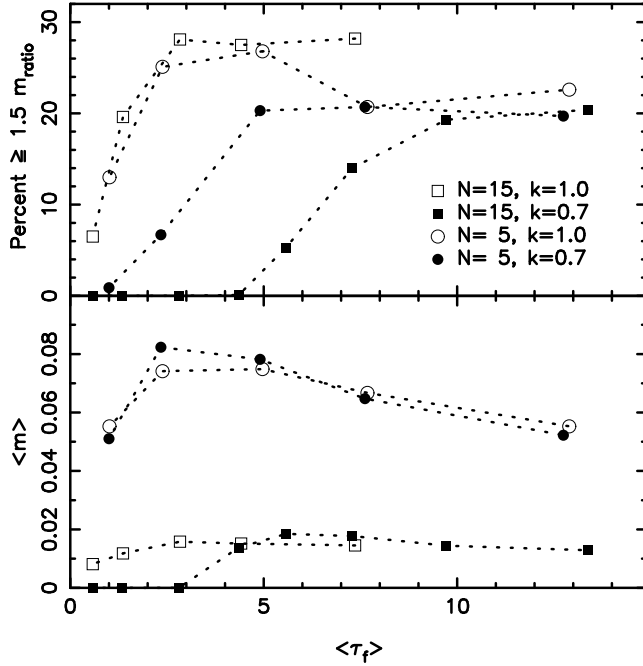


Fig. 4.— Top panel shows the percentage of 1000 runs where the fractional polarization ratio,  $m_{ratio}$  between  $\lambda^2 = 2.0$  and  $\lambda^2 = 1.0$  is  $\geq 1.5$  indicating significant inverse depolarization. Integrated results from cubes of random field of dimensions  $5 \times 5 \times 5$  and  $15 \times 15 \times 15$  are plotted with and without a moderate shock where unit length has been shortened to length  $k$  along the jet axis (Wardle et al. 1994). Each case is plotted for a variety of mean Faraday depths,  $\langle \tau_f \rangle$ . The bottom panel shows the mean fractional polarization at the longest wavelength for the runs where  $m_{ratio} \geq 1.5$ .